Journal of Materials Research and Technology 34 (2025) 2828–2835

Contents lists available at ScienceDirect

Journal of Materials Research and Technology

journal homepage: www.elsevier.com/locate/jmrt

Tunable structuring of nanocellulose-based sustainable lubricants by an external electric field

Samuel D. Fernández-Silva, Miguel A. Delgado *, María García-Pérez, Claudia Roman, Moisés García-Morales

Departamento de Ingeniería Química, Química Física y Ciencias de Los Materiales. Centro de Investigación en Tecnología de Productos y Procesos Químicos (Pro2TecS), Campus de "El Carmen", Universidad de Huelva, 21071, Huelva, Spain

ARTICLE INFO

Handling editor: P.Y. Chen

Keywords:
Nanocellulose
Lubricant
Electrorheology
Oscillatory shear
Optical microscopy analysis

ABSTRACT

This research investigates the morphological and electrorheological (ER) behaviors of nanocellulose-based lubricants. Commercial fibrillated (CNF) and crystalline (CNC) nanocelluloses were dispersed in castor oil, at two selected concentrations of 1 and 4 wt%, to obtain fully sustainable electro-active lubricants. Small amplitude oscillatory shear (SAOS) tests were performed within the linear viscoelastic (LVE) range to investigate the rheological behavior induced by the combined effect of pre-shear and voltage. Hence, prior to the SAOS tests at electric field intensities ranging from 0 to 4 kV/mm, the samples were subjected to simple shear, at two selected values of 0.1 and 30 s^{-1} and for 5 min, under the same voltages. A portable digital microscope, attached to a strain-controlled rheometer, allowed visualizing the electro/shear-induced structuring of the lubricants and establishing relationships with their rheological response. In general, both storage and loss moduli were found to change with the electric field. Regarding the effect of nanocellulose concentration, the formation of thin strings was observed at 1 wt% nanocellulose when the lubricant was subjected to low pre-shear. Their angular displacement increased with the electric field. On the contrary, at 4 wt% nanocellulose, a fully entangled network was perceived, such that the nanofiber rotation was severely restrained. The highest pre-shear yielded a structural break which, under the action of an electric voltage, enabled the formation of a different structural conformation when pre-shear halted, in comparison with the lowest pre-shear. Such event led to a notorious reduction in both storage and loss moduli, mainly at the lowest electric field intensities.

1. Introduction

In terms of friction and wear reduction, the main strategy of the lubricant sector over the last decades has been merely promoting a "passive" improvement in the lubricant performance by using potentially hazardous additives [1]. Fortunately, the rise in environmental awareness is driving the replacement of such additives as well as the mineral/synthetic base oils used with non-toxic, renewable and sustainable substances. As such, both scientific community and manufacturers are making great efforts for the sake of developing fully environmentally respectful bio-based lubricants [2].

Recently, "smart materials" have attracted great interest for cutting-edge applications. In general, they can be described as materials which respond or adapt to a specific external stimulus [3]. There are multiple examples in literature, such as piezoelectric parts, shape memory alloys or electro- and magneto-rheological fluids [3]. Among these, electro-rheological (ER) fluids are of special relevance in the fields of composites, clutches, valves, dampers, shock absorbers or lubricants, in several industries such as automotive, marine or robotics [3–8]. ER fluids are suspensions commonly composed of electrically polarizable particles dispersed in a non-conductive liquid. Under an electric potential, particles polarize and align, yielding chain-like structures parallel to the direction of the electric field [9,10], thereby increasing their apparent viscosity by up to several orders of magnitude [5]. It is noteworthy that the polarized particle morphology strongly affects the structuring process of an electrified suspension and, consequently, also affects the impact of the hydrodynamic forces on the suspension rheological behavior [11–13]. In addition, when this stimulus ceases, the effect is reversed with a response time as short as a few milliseconds [14]. This phenomenon has recently woken up special interest in the

* Corresponding author.
E-mail addresses: samuel.fernandez@diq.uhu.es (S.D. Fernández-Silva), miguel.delgado@diq.uhu.es (M.A. Delgado), maria.gperez@diq.uhu.es (M. García-Pérez), claudia.roman@diq.uhu.es (C. Roman), moises.garcia@diq.uhu.es (M. García-Morales).

https://doi.org/10.1016/j.jmrt.2024.12.183
Received 14 October 2024; Received in revised form 17 December 2024; Accepted 22 December 2024
Available online 28 December 2024

lubrication field, as a way of promoting an "active" improvement in the lubricant performance [10,15–17], given the outstanding impact that on-demand friction control by an electric potential may catalyze.

The development of innovative and environmentally friendly bio-based lubricants entails a remarkable source of research nowadays. In this sense, lignocellulosic biomass, the most abundant biopolymers on our planet, has emerged as a prominent raw material within the lubricant field as a natural, non-toxic, renewable and biodegradable resource [18–20]. For the specific case of lubricants, just to name a few, Cortés Triviño et al. [21] studied formulations based on castor oil and epoxidized cellulose pulp, whose performance depended on the degree of modification of the cellulose pulp and the epoxide compound used. Li et al. [22] observed good stability and a reduction in the friction coefficient of 30 % when adding cellulose nanocrystals at 2 wt% in a polyalphaolefin base oil. Roman et al. [23] have shown that an oleogel based on 1.4 wt% cellulose nanofibers in castor oil has a viscoelastic behavior very similar to a commercial lubricating grease (8 wt% lithium soap thickener) with a comparable NLGI (National Lubricating Grease Institute) consistency. Fernández-Silva et al. [24] reported the excellent tribological performance of 3.3 wt% nanocellulose in vegetable oil dispersions, which yielded very remarkable wear scar diameter reductions while Delgado-Canto et al. [10] introduced the use of nanocellulose in electrorheology based smart lubricants. However, the great potential of exploitation of lignocellulosic materials still remains unexplored within the lubricant technology field.

Cellulose nanofibers can be obtained by either purely mechanical or combined chemical/mechanical treatment of the cellulose pulp [9]. They have varying diameters and length, depending on the cellulose source and treatment applied for their production [25]. Cellulose nanofibers are composed of a string of successive cellulose nanocrystals, linked by amorphous domains [9,18]. Cellulose nanocrystals are obtained by acid hydrolysis of such amorphous domains, which causes the hydrolytic cleavage of the glycosidic bonds and the consequent release of individual crystallites after mechanical treatment [18,26]. Both cellulose types have an identical composition, with crystallinity and aspect ratio being their main differentiating factors [18].

A very noteworthy feature of cellulose fibers, both micro and nano, is their capacity to be polarized and arranged into columnar structures by an electric field [10,27–30]. Kadimi et al. [31] developed an interesting study on the effect of the aspect ratio and charge of cellulose nanofibers and nanocrystals on their alignment under AC electric field. Moreover, electrorheological characterizations are found in literature, in relation to nanocellulose-based composites or fluids [9,10,27]. Even so, to the best of our knowledge, there are hardly any studies that analyze the combined influence of shear and electric field on their tunable structuring. Furthermore, none of these studies explore the connections between various structural configurations and their rheological behavior using in-situ optical microscopy visualization. In relation to lubricants, the authors have previously reported a qualitative model grounded on the evaluation of viscous flow measurements and theoretical considerations. It was also described how it can benefit the friction behavior of these nanocellulose-based sustainable lubricants under an external electric field [10]. Based on that work, we herein hypothesize that, in the presence of an electric field, the structural conformation of nanocellulose (also micro) in a vegetable oil strongly depends on both concentration and applied shear rate. Thus, the present paper has placed a particular emphasis on obtaining clear visual evidence of how the dielectrophoretic and hydrodynamic forces compete for the orientation of the nanocellulose particles in a vegetable oil suspending medium. For this purpose, oscillatory shear tests allowed a comparative analysis of the mechanical strength of the nanocellulose structures to be conducted, under specific pre-shear and voltage conditions. As a novelty, the in-situ optical microscopy visualization revealed how the structuring of polarized nanocellulose particles is affected by the external electric field and the shear rate conditions. These findings could be of particular relevance in the development of "smart" bio-based lubricants, whose friction behavior will greatly depend on the way the particulate phase arranges within the oily phase. More transversally, the knowledge gained from this study could even be extended to nanocellulose-based composite fabrication, where tailored orientation of the nanofibers might be demanded.

2. Materials and methods

2.1. Materials

Commercial crystalline (CNC) and fibrillated (CNF) nanocelluloses were purchased from Nanografi Co. Ltd. (Jena, Germany). As per specifications, CNF was mechanically obtained from cotton cellulose pulp and dehydrated by drying process. Previously, the pulp had been modified by carboxymethylation (COOH content of 1178 ± 37 μmol/g). CNC was obtained by sulfuric acid hydrolysis (sulphate groups are present). CNF and CNC basically differ in crystallinity and aspect ratio. CNC has a diameter of 10–20 nm, length of 0.3–0.9 μm and 100 % crystallinity (by x-ray diffraction, XRD). On the other hand, CNF has the same diameter, length of 2–3 μm and 92 % crystallinity by XRD. It is worth pointing out that the drying process of these commercial cellulose nanoparticles can lead to the formation of agglomerates. This happens because when the moisture is removed, the particles have a tendency to stick together. Therefore, this agglomeration may present difficulties when attempting to disperse these particles in the base oil [32]. For that reason, both cellulose micro and nanofibers were found in all the nanocellulose-based dispersions that were studied.

Castor oil (CO) purchased from Guinama (Spain), with dynamic and kinematic viscosities of 550 mPa s and 574 cSt, respectively, at 25 °C, was employed as the dispersing medium. Extensive literature regarding castor oil as a raw material [33] and as a lubricant basestock [34] can be found elsewhere.

2.1.1. Preparation of nanocellulose-based dispersions

CNF and CNC in castor oil dispersions were prepared, at selected concentrations of 1 and 4 wt%, using a two-step methodology. The celluloses were first coarsely dispersed in castor oil through magnetic stirring for 30 min at 50 °C. Subsequently, fine dispersion was achieved by using an UP400St ultrasonic homogenizer (Hielscher, Germany). The total energy input was 7 Wh, and the temperature was always maintained below 80 °C by placing the container in an ice bath. The samples were ultrasonicated for 5 min before the tests, to ensure completely homogeneous dispersions.

2.2. Small amplitude oscillatory shear (SAOS) test and visual inspection by optical microscopy

Small amplitude oscillatory shear (SAOS) tests were carried out on a strain-controlled rheometer, model ARES-G2 (TA Instruments, USA) within a frequency range of 10^{-2} to 10^{2} rad/s. Previously, the linear viscoelastic (LVE) range was determined by strain sweep tests at 6.28 rad/s. A Keysight 33210A current generator (Agilent, USA) and a Trek 609E-6 high voltage power amplifier (Trek, Inc., USA) coupled to this rheometer enabled to apply the required electric voltages.

Smooth plate-plate geometry of 25 mm diameter and 0.5 mm gap was used for the whole testing procedure at room temperature (ca. 25 °C). Before conducting the SAOS tests, the fluids were subjected to pre-shear of 0.1 or 30 s^{-1} (referred to as "low PS" and "high PS", respectively, hereinafter) for 5 min. According to a previous study carried out by Delgado et al. [10], such two values have been selected as representatives of shear rate at which the electric current varies significantly, thereby suggesting differences in the chain-like structures formed. The SAOS tests (including the pre-shear step) were performed under selected electric fields of 0.16, 0.8, 2.4 and 4 kV/mm.

While running the rheological measurements, a portable optical microscope (Fig. 1) enabled to record the micro and nanocellulose

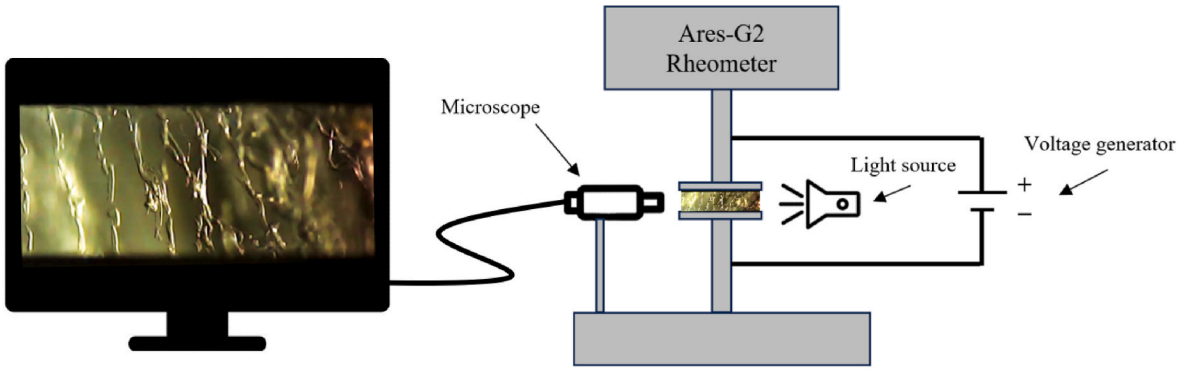

Fig. 1. Schematics of the experimental set-up used for the optical visualization of nanocellulose structures.

structures arisen between the parallel plates (electrodes). A light source was set opposite to the microscope, pointing at the lubricant contained between the measuring parallel plates. Such experimental set-up allowed for an in-situ visual inspection of the electro-induced structural conformation of the nanocelluloses under selected voltages and shear rate values.

3. Results and discussion

3.1. Optical microscopy analysis of the electro-active structuring of nanocellulose in castor oil

Delgado et al. [10] previously reported a theoretical model describing the potential competition between the hydrodynamic (shear stress) and dielectrophoretic (electric field) forces that control the way nanocellulose arranges in vegetable oil dispersions. Based on that, under quiescent conditions, cellulose nanofibers would polarize and align parallel to the direction of the electric field (i.e. perpendicular to the measuring plates), forming chain-like or string structures under a certain voltage difference. On the other hand, when the electric field is off, single cellulose nanofibers being subjected to shear would orient in the flow direction (i.e., parallel to the plates' surface). Furthermore, electrostatic forces between interfacially polarized cellulose particles would enhance their shear resistance, thereby increasing their yield stress and viscoelastic moduli with increasing voltage values [10,35]. This will be discussed later below.

Further to such theoretical considerations, we aimed to contrast the origin and glimpse the individual contribution of each of the mechanisms that are presumed to cause the modification of the lubrication process under electric field. Fortunately, our home-made experimental set-up allowed collecting conclusive visual evidence on the specific role of the driving forces competing in the aforementioned structuring mechanism. Hence, the nanocellulose-based dispersions were subjected to specific voltage differences, while being exposed to shear rates of 0.1 and 30 s^{-1} for 5 min. Figs. 2 and 3 depict representative optical micrographs of polarized CNF and CNC particle structures, respectively. Pictures were captured at the edge of the parallel plate measuring cell (where the light path is the shortest and the image is the clearest), immediately after the pre-shear step was completed. In most cases, at the highest voltages, bubbling prevented nice images from being taken [36].

In general, the applied voltage drove a quick alignment of neighboring polarized CNF and CNC particles in the electric field direction. At a concentration of 1 wt%, chain-like structures are distinctly visible at every applied voltage. As observed in Figs. 2 and 3, at a shear rate of 0.1 s^{-1}, the chain-like structures formed upon application of the electric field were strong enough so as to withstand the effect of pre-shear. In other words, the dielectrophoretic forces resulting from the electric field were able to keep the polarized cellulose strings nearly intact against the hydrodynamic forces at low shear rates. This result also reveals the high interfacial polarization capacity of cellulose [37–39]. Even so, a slight

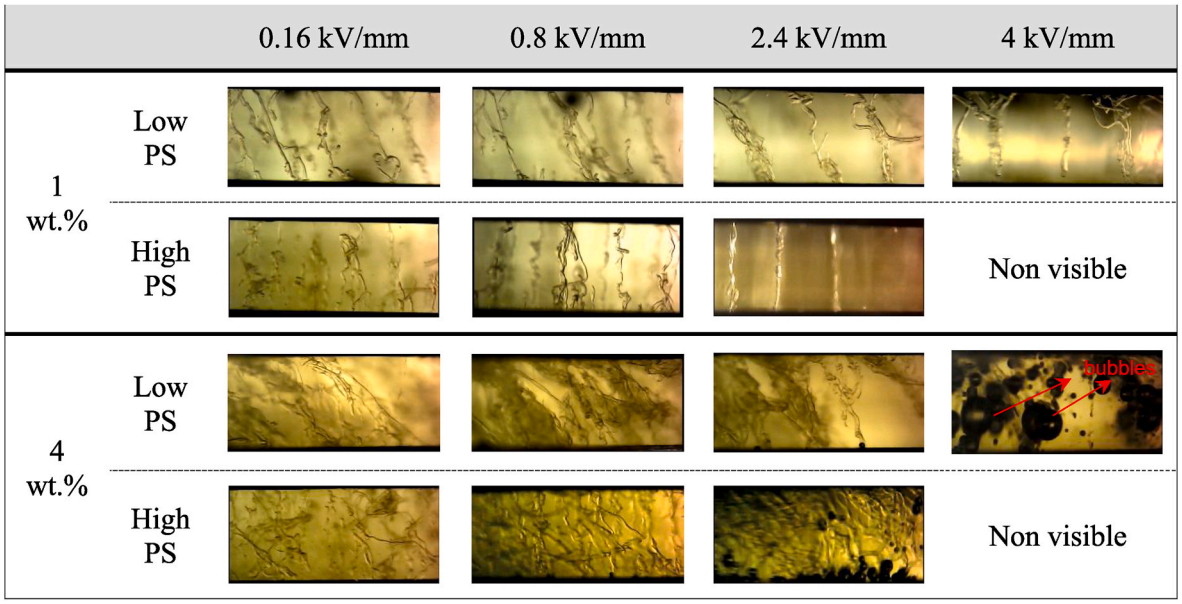

Fig. 2. Optical microscopy visualization for 1 and 4 wt% CNF-based dispersions under the combined effect of electric field and pre-shear.

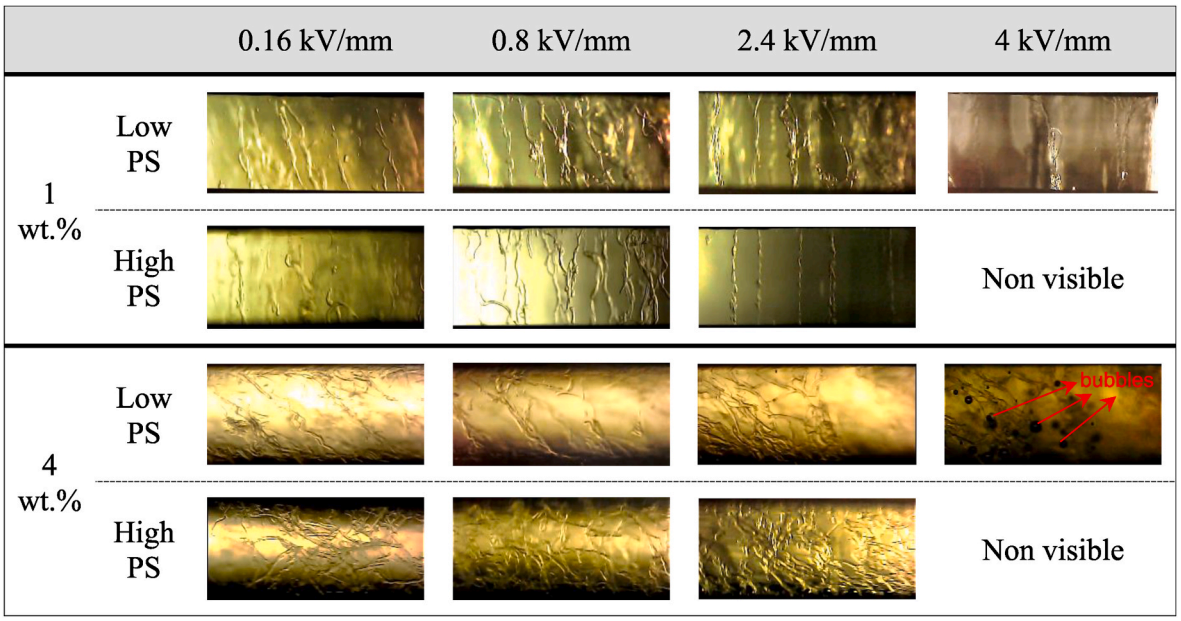

Fig. 3. Optical microscopy visualization for 1 and 4 wt% CNC-based dispersions under the combined effect of electric field and pre-shear.

inclination in the flow direction was observed at electric field values below 2.4 and 0.8 kV/mm for CNF-based and CNC-based dispersions, respectively.

It is noteworthy to retrieve the Newton's Law of viscosity, in terms of velocity profile [40]. When a certain torque is applied to the moving bottom plate to initiate movement at a constant rotational speed, a shear stress profile arises within the fluid confined between the two parallel surfaces. The shear stress generates a velocity profile, with the fluid layer in the immediate vicinity of the bottom surface moving at the highest speed. As we go upward through the fluid in the vertical direction, every of the following fluid layer moves at a slightly lower velocity than the preceding layer, until zero velocity is reached just below the non-moving upper plate. Consequently, the lower end of the chain-like structures was subjected to the highest velocity, which caused their observed tilting.

It can be clearly appreciated that, under low PS, the higher electric field intensity, the lower the inclination of the polarized nanocellulose was. Moreover, the larger the length of the nanocellulose particle (CNF is longer than CNC), the lower the angular displacement was (e.g. 71.8° vs 78.9° for CNF and CNC at 0.8 kV/mm, respectively). This result would suggest a more effective stress transfer along a chain formed by the longest particles. Even so, such an observed effect of the hydrodynamic forces was not too large.

For comparison purposes, all optical images were processed with the open-source Java-based graphic program, ImageJ. A convolution filter was applied and the angular displacement (rotation angle provoked by a torque that tends to line up the polarized rod-like particle with the electric field) of the cellulose chain-like structures relative to the bottom plate was measured. Calculated values, in terms of average and standard deviation, are provided in Table 1. At low concentrations, the angular displacement increased with voltage. At electric fields of 4 and 2.4 kV/mm, the nanocellulose chain-like arrangements aligned fully parallel to the electric field, i.e., forming an angle of ca. 90° relative to the bottom plate. It can be, thereby, concluded that particles are capable of offsetting the effect of the hydrodynamic forces at the lowest shear rate. Hence, it can also be stated that, under such conditions, the structural conformation of the nanocellulose chains was prevailingly influenced by the dielectrophoretic forces. Additionally, those chains became thicker with time during the pre-shear step, which is consistent with the findings reported by Kadimi et al. [31], due to the continuous branching of free cellulose particles in already formed chains.

Table 1
Angular displacement of the cellulose chain-like structures under the combined effect of electric field (0.16–4 kV/mm) and pre-shear (at 0.1 and 30 s^{-1}) for 1 and 4 wt% CNF and CNC-based dispersions.

	0.16 kV/mm	0.8 kV/mm	2.4 kV/mm	4 kV/mm
CNF-based dispersions				
1 wt% low PS	68.1 ± 0.5°	71.8 ± 2.3°	74.5 ± 2.1°	86.8 ± 2.4°
1 wt% high PS	90°	90°	90°	Non visible
4 wt% low PS	46.4 ± 1.7°	53.7 ± 3.7°	63.1 ± 4.7°	Bubbling
4 wt% high PS	Entangled Network			Non visible
CNC-based dispersions				
1 wt% low PS	72.5 ± 3.1°	78.9 ± 4.1°	85.9 ± 1.6°	90°
1 wt% high PS	90°	90°	90°	Non visible
4 wt% low PS	42.0 ± 0.5°	47.6 ± 0.5°	52.4 ± 8.9°	Bubbling
4 wt% high PS	Entangled Network			Non visible

In contrast, high PS (30 s^{-1}) prevented the chain-like structures induced by the dielectrophoretic forces from being initially formed. CNF and CNC rod-like particles were seen to orient in the flow direction during the pre-shear step, thereby appearing as lamellar structures. A video is provided as supplementary information, for the sake of clarity. Clear evidence of such an effect was found at the lowest electric field, 0.16 kV/mm, for the highly concentrated dispersion, 4 wt%. Due to steric hindrance, its lamellar arrangement behavior remained for some time once shear had ceased. As previously noted by Delgado et al. [10], the rotation effect provoked by the electric field could be hindered by the formation of such lamellar structures due to the interaction of adjacent nanocellulose rod-like particles by non-polarization forces, such as intermolecular H-bond or van der Waals forces. Such interactions involve the –OH groups present in both CNF and CNC, as well as those in the ricinoleic fatty acid molecule of castor oil. As a result, the orientation of the polarized particles along the electric field was constrained during the pre-shear step. In the case of 1 wt% dispersions, upon shear ceased, the polarized CNF and CNC particles suddenly aligned along the electric field, forming in most cases 90°-pitched chain-like structures, as observed in Figs. 2 and 3. It is noteworthy that electric fields of 0.16 kV/mm or even 0.8 kV/mm were not high enough for the particles to immediately align after the high PS step. Hence, some strings remained isolated, failing to bridge the two electrodes for some minutes. In contrast, at and above 2.4 kV/mm, the chain-like structures formed instantaneously after shear ceased. We can conclude that under

sufficiently strong hydrodynamic forces, electric field-triggered orientation can be delayed or even suppressed, depending on the dispersion concentration.

It is worth noting that the number of chains observed diminished with shear rate and voltage. This outcome is very well appreciated, for example, in the case of 1 wt%, under high PS and at 2.4 kV/mm. In that sense, micrographs displayed in Figs. 2 and 3 were acquired at the edge of the plate-plate geometry, where the light intensity through the sample was the highest. As reported by Parker [41], the electric field lines arisen between two oppositely charged finite parallel plates are perpendicular to their surface, but they curve outwards at the edges. This leads to a reduction in the magnitude of the electric field near the edges of the plate-plate geometry, which may account for the decrease in the number of chain-like structures observed at high shear rate and voltage. At the lowest shear rate, 0.1 s^{-1}, the hydrodynamic forces were not powerful enough to overcome the electrostatic forces that linked the polarized particles together. Consequently, the chain-like structures formed along the electric field direction offered some resistance against flowing towards the inner part of the plate-plate geometry. However, due to the high shear, disrupted chains were drawn inwards in the confining gap, where the electric field is more intense. This effect was particularly noticeable at 4 kV/mm at 0.1 s^{-1}, and 2.4 kV/mm at 30 s^{-1}, for both nanocellulose-based dispersions at 1 wt%.

In turn, the most concentrated dispersion, 4 wt%, followed a very contrasting morphology pattern, approaching progressively to a complete entangled network with increasing electric field intensity at high pre-shear. At 0.1 s^{-1} and electric field of 0.16 kV/mm, chain-like structures are fairly visible in the electric field direction, even though some of them started to branch by grafting other neighboring chains. Furthermore, the angular displacement values of these chains were markedly lower than those observed for 1 wt% (Table 1). This is due to the greater effect of shear on the orientation of such type of microstructures. Due to the evident steric hindrance, the angular displacement was lower than at 1 wt%, because the branched structures found more difficulties to orient parallel to the electric field under the effect of shear. At 0.8 kV/mm and higher voltages, polarized CNF and CNC particles started to arrange into a percolated 3D network and, thereby, separate columnar structures were less evident. At the highest shear rate, the intermolecular forces previously commented among fully flow-oriented nanocellulose strings yielded lamellar structures. At 0.16 kV/mm, the strong steric hindrance hampered their alignment along the electric field lines. By way of example, Fig. 3 displays poorly electric field-oriented lamellar structures (low angular displacement). Interestingly enough, higher voltages turned such structures into a fully entangled network. These findings match the outcomes reported in Delgado et al. [10], where remarkably differences in the viscous flow behavior in an electrified measuring cell were noticed with dispersion concentration. In-situ optical inspection has confirmed the reported hypothesis on a network-like structuring pattern at concentrations higher than 2 wt% nanocellulose.

3.2. Combined effect of pre-shear and electric field on the SAOS behavior

The electro-active structuring of the dispersions studied is directly related to the inherent interfacial polarization capacity of nanocellulose and the consequent electrorheological effect [10,12,37]. In order to better understand how the combined effect of hydrodynamic forces (shear rate) and dielectrophoretic forces (electric field) may affect their ER behavior, the nanocellulose-based dispersions were subjected to frequency sweep tests, from 10^{-2} to 10^{2} rad/s, within the linear

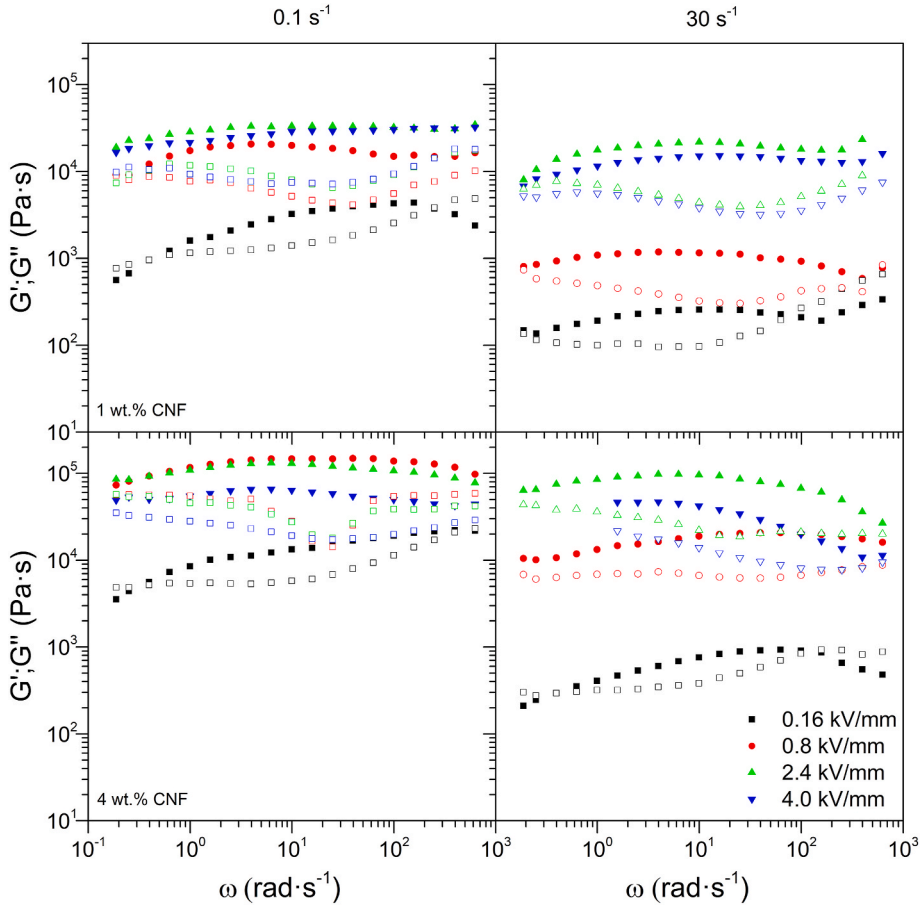

Fig. 4. Storage (filled symbols) and loss (empty symbols) moduli of SAOS measurements conducted on CNF-based dispersions at 1 wt% (top) and 4 wt% (bottom).

viscoelastic (LVE) range. Previously, the samples were pre-sheared at 0.1 or 30 s^{-1} for 5 min. As can be observed in Figs. 4 and 5, the results of SAOS tests conducted on CNF and CNC-based dispersions, respectively, exhibited a comparatively similar behavior within the LVE range. In the absence of voltage, their purely viscous behavior prevented them from being measured. However, the evolution of the linear viscoelastic moduli with frequency induced by the electric field was quite similar to that found for traditional lithium lubricating greases [42]. Such behavior is characterized by a higher, and sometimes nearly constant, value of the storage modulus (G') and a minimum in the loss modulus (G'') at intermediate frequencies, which is an intrinsic feature of microstructured systems.

Outstanding variations were observed with the electric field. At the lowest electric field intensity, the limits of the plateau region (crossover points) are found, in general, in the frequency range evaluated, regardless of concentration and pre-shear. When the electric field was increased, the plateau region progressively extended, and its limits (low, high, or both) fell outside the studied frequency interval. As long as concentration is concerned, the plateau region also expanded with increasing concentration. These effects are due to the stiffness of the nanocellulose structural conformations which, as previously depicted in Figs. 2 and 3, increased with both voltage and concentration.

In general terms, both storage and loss moduli typically increased with voltage. This indicates that the nanocellulose arrangements gained progressively consistency with the electric field. This increased consistency again reflects the influence of the electrostatic forces between the interfacially polarized cellulose nanofibers or nanocrystals as the voltage was raised. As a result, these chain-like structures, aligned in the electric field direction, became stronger and thicker with the electric field strength (see Figs. 2 and 3) [43].

More specifically, the effect of voltage on the ER behavior of these nanocellulose-based dispersions was influenced by both concentration and pre-shear. In that sense, at 1 wt%, an asymptotic trend with the electric field was observed. When a pre-shear of 0.1 s^{-1} was applied, the asymptotic limit was nearly reached at an electric field value as low as 0.8 kV/mm. However, when the pre-shear was increased to 30 s^{-1}, such limit shifted to a higher electric field value, up to 2.4 kV/mm. Therefore, at the highest shear rate, lower electric field values were not strong enough to immediately bridge the upper and lower plates with nanocellulose strings (see Figs. 2 and 3). This event resulted in less structural consistency, which was denoted by lower viscoelastic moduli values. Moreover, as previously mentioned, the attraction of the polarized nanocellulose particles towards the central part of the parallel plates at high electric fields induced changes in the structural distribution all over the measuring area. This event also affected the observed reduction in the viscoelastic moduli. At 4 wt%, the storage and loss moduli increased with increasing the electric field up to 2.4 kV/mm, and then decreased at 4 kV/mm. As previously mentioned, an electric field of 4 kV/mm was seen to produce a severe bubbling effect, much more noticeable at 4 wt% than at 1 wt%. Hence, bubbling might be the reason behind the reduction in the storage and loss moduli at 4 wt%, which is observed in Figs. 4 and 5.

4. Conclusions

The tunable electro-active structuring of nanocellulose in vegetable oil was feasible by combining voltage and shear. In general, the applied voltage led to a rapid alignment, in the electric field direction, of neighboring polarized nanocellulose particles. At the lowest concentration studied, i.e. 1 wt%, chain-like structures were clearly observed

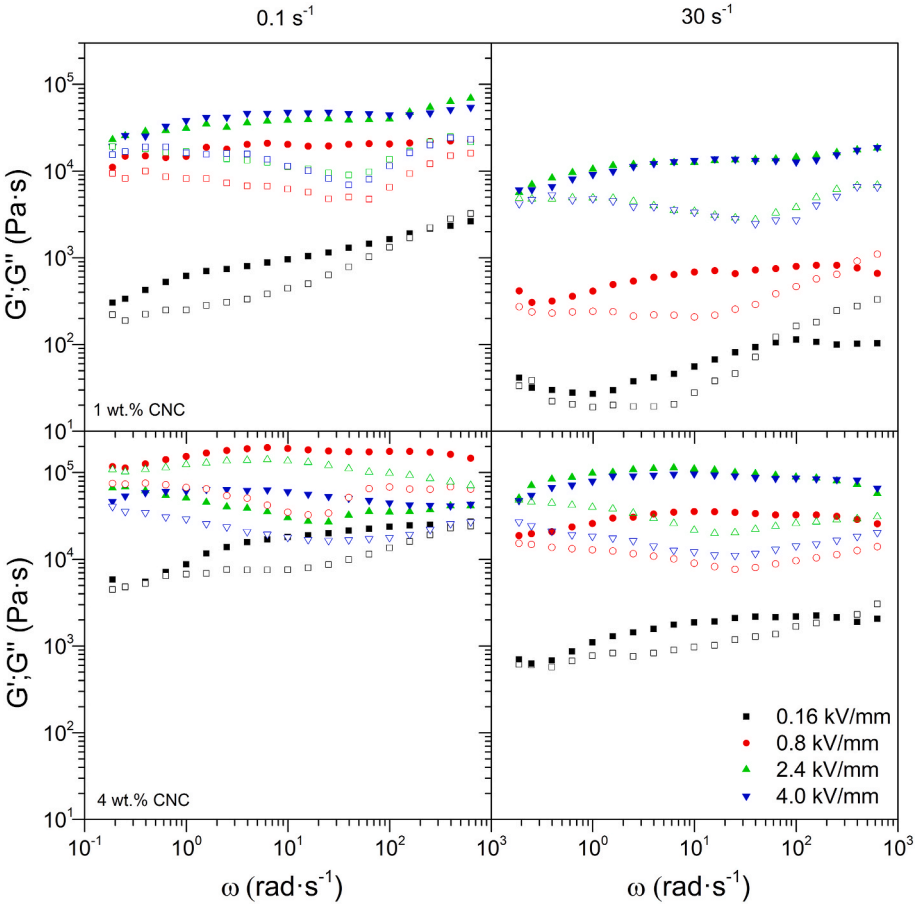

Fig. 5. Storage (filled symbols) and loss (empty symbols) moduli of SAOS measurements conducted on CNC-based dispersions at 1 wt% (top) and 4 wt% (bottom).

within the entire voltage interval applied. As such, the dielectrophoretic effect due to the presence of an electric field was powerful enough so as to hold the polarized cellulose particles together under the action of low hydrodynamic forces (shear rate of 0.1 s^{-1}). Even so, the arisen chain-like structures, mainly those from cellulose nanofiber, slightly tilted in the flow direction at the lowest electric fields. However, under the highest shear rate studied of 30 s^{-1}, the formation of nanocellulose strings was disrupted in such a way that, at 0.16 kV/mm, they were unable to immediately align and bridge the upper and lower measuring plates. In consequence, a very remarkable reduction in the linear viscoelastic moduli was perceived.

In turn, at the highest concentration, i.e. 4 wt%, the polarized particles were prevented from being arranged into the aforementioned alignment due to the formation of more complex structures which constrained their angular displacement. Hence, large lamellar conformations were observed as a consequence of intermolecular forces other than interfacial polarization interactions. Only at a shear rate as small as 0.1 s^{-1} and at the lowest electric field values were the chain-like structures visible, even though some of them began to branch out. Moreover, as compared to the much simpler structures at 1 wt%, such branched structures appeared to be more sensitive to shear stress, as denoted by markedly lower angular displacements. At the highest shear rate, in a similar way to the 1 wt% dispersion, polarized CNF and CNC particles oriented in the flow direction during the pre-shear step. However, when the pre-shear ceased, the nanocellulose particles formed a fully entangled network. Chain-like structures were, then, barely observable.

The reported outcomes may have outstanding practical implications. As far as friction and wear in lubricated contacts are concerned, our findings would involve a prospective use of electric potentials in order to adapt the in-service performance of smart sustainable lubricants to changing working conditions. More transversally, the knowledge gained from the present study may provide a valuable insight into the electro-triggered control of the in-situ orientation of cellulose nanofibers in molten or curable matrices. This may find application as an alternative to other mechanical techniques with a view to achieving high strength cellulose-reinforced composite materials, or even as a strategy to minimize their percolation threshold.

CRediT authorship contribution statement

Samuel D. Fernández-Silva: Methodology, Validation, Investigation, Writing – original draft. **Miguel A. Delgado:** Conceptualization, Methodology, Writing – review & editing, Supervision, Project administration, Funding acquisition. **María García-Pérez:** Validation, Investigation. **Claudia Roman:** Validation, Investigation. **Moisés García-Morales:** Conceptualization, Methodology, Resources, Writing – review & editing, Project administration, Funding acquisition.

Funding sources

This work is part of three Research Projects: two of them sponsored by "University of Huelva" in 2024 (EPIT1312023 and EPIT16142023 (Programa Operativo FEDER Andalucía 2021-2027)) and another research project (PID2023-151761NB-I00) sponsored by the CIENCIA-FEDER I + D + i Spanish Programme. The authors gratefully acknowledge their financial support.

Declaration of competing interest

The authors declare that they have no known competing financial interests or personal relationships that could have appeared to influence the work reported in this paper.

Abbreviations

CNF	cellulose nanofiber
CNC	cellulose nanocrystal
ER	electro-rheology
LVE	linear viscoelastic
PS	pre-shear
SAOS	small amplitude oscillatory shear

Appendix A. Supplementary data

Supplementary data to this article can be found online at https://doi.org/10.1016/j.jmrt.2024.12.183.

References

[1] Danilov AM, Bartko RV, Antonov SA. Current advances in the application and development of lubricating oil additives. Petrol Chem 2021;61:35–42. https://doi.org/10.1134/S0965544121010035.
[2] Saxena A, Kumar D, Tandon N. Development of lubricious environmentally friendly greases using synergistic natural resources: a potential alternative to mineral oil-based greases. J Clean Prod 2022;380. https://doi.org/10.1016/j.jclepro.2022.135047.
[3] Bahl S, Nagar H, Singh I, Sehgal S. Smart materials types, properties and applications: a review. In: Mater today proc. Elsevier; 2020. p. 1302–6. https://doi.org/10.1016/j.matpr.2020.04.505.
[4] Liu YD, Choi HJ. Electrorheological fluids: smart soft matter and characteristics. Soft Matter 2012;8:11961–78. https://doi.org/10.1039/c2sm26179k.
[5] Winslow WM. Induced fibration of suspensions. J Appl Phys 1949;20:1137–40. https://doi.org/10.1063/1.1698285.
[6] Coulter JP, Weiss KD, Carlson JD. Engineering applications of electrorheological materials. J Intell Mater Syst Struct 1993;4:248–59. https://doi.org/10.1177/1045389X9300400215.
[7] Barber GC, Jiang QY, Zou Q, Carlson W. Development of a laboratory test device for electrorheological fluids in hydrostatic lubrication. Tribotest 2005;11:185–91. https://doi.org/10.1002/tt.3020110302.
[8] García-Morales M, Fernández-Silva SD, Roman C, Delgado MA. Electro-active control of the viscous flow and tribological performance of ecolubricants based on phyllosilicate clay minerals and castor oil. Appl Clay Sci 2020;198:105830. https://doi.org/10.1016/j.clay.2020.105830.
[9] Kadimi A, Benhamou K, Habibi Y, Ounaies Z, Kaddami H. Nanocellulose alignment and electrical properties improvement. In: Multifunctional polymeric nanocomposites based on cellulosic reinforcements. William Andrew Publishing; 2016. p. 343–76. https://doi.org/10.1016/B978-0-323-44248-0.00011-0.
[10] Delgado-Canto MA, Fernández-Silva SD, Roman C, García-Morales M. On the electro-active control of nanocellulose-based functional biolubricants. ACS Appl Mater Interfaces 2020;12:46490–500. https://doi.org/10.1021/acsami.0c12244.
[11] Tsuda K, Takeda Y, Ogura H, Otsubo Y. Electrorheological behavior of whisker suspensions under oscillatory shear. Colloids Surf A Physicochem Eng Asp 2007;299:262–7. https://doi.org/10.1016/j.colsurfa.2006.11.050.
[12] Yin J, Zhao X, Xia X, Xiang L, Qiao Y. Electrorheological fluids based on nanofibrous polyaniline. Polymer 2008;49:4413–9. https://doi.org/10.1016/j.polymer.2008.08.009.
[13] Wu J, Jin T, Liu F, Guo J, Cui P, Cheng Y, Xu G. Preparation of rod-like calcium titanyl oxalate with enhanced electrorheological activity and their morphological effect. J Mater Chem C Mater 2014;2:5629–35. https://doi.org/10.1039/c4tc00691g.
[14] Seo YP, Choi HJ, Seo Y. Analysis of the flow behavior of electrorheological fluids with the aligned structure reformation. Polymer 2011;52:5695–8. https://doi.org/10.1016/j.polymer.2011.10.033.
[15] Luo JB, Shen MW, Wen SZ. Tribological properties of nanoliquid film under an external electric field. J Appl Phys 2004;96:6733–8. https://doi.org/10.1063/1.1806259.
[16] Dimarogonas AD, Kollias A. Electrorheological fluid-controlled "smart" journal bearings. Tribol Trans 1992;35:611–8. https://doi.org/10.1080/10402009208982163.
[17] Choi SB, Sohn JW, Han YM, Lee CH. Wear characteristics under boundary lubrication contacts in phosphorated starch-based electrorheological fluid. Tribol Trans 2010;53:256–65. https://doi.org/10.1080/10402000903312331.
[18] Dufresne A. Nanocellulose: from nature to high performance tailored materials. De Gruyter Mouton; 2012. https://doi.org/10.1515/hf-2013-0027.
[19] Shi Z, Phillips GO, Yang G. Nanocellulose electroconductive composites. Nanoscale 2013;5:3194–201. https://doi.org/10.1039/c3nr00408b.
[20] Trache D, Tarchoun AF, Derradji M, Hamidon TS, Masruchin N, Brosse N, Nanocellulose MH Hussin. From fundamentals to advanced applications. Front Chem 2020;8. https://doi.org/10.3389/fchem.2020.00392.
[21] Cortés-Triviño E, Valencia C, Delgado MA, Franco JM. Thermo-rheological and tribological properties of novel bio-lubricating greases thickened with epoxidized lignocellulosic materials. J Ind Eng Chem 2019;80:626–32. https://doi.org/10.1016/j.jiec.2019.08.052.

[22] Li K, Zhang X, Du C, Yang J, Wu B, Guo Z, Dong C, Lin N, Yuan C. Friction reduction and viscosity modification of cellulose nanocrystals as biolubricant additives in polyalphaolefin oil. Carbohydr Polym 2019;220:228–35. https://doi.org/10.1016/j.carbpol.2019.05.072.
[23] Roman C, García-Morales M, Eugenio ME, Ibarra D, Martín-Sampedro R, Delgado MA. A sustainable methanol-based solvent exchange method to produce nanocellulose-based ecofriendly lubricants. J Clean Prod 2021;319:128673. https://doi.org/10.1016/j.jclepro.2021.128673.
[24] Fernández-Silva SD, Delgado MA, Roman C, García-Morales M. Rheological and tribological properties of nanocellulose-based ecolubricants. Nanomaterials 2021; 11:2987. https://doi.org/10.3390/nano11112987.
[25] Copenhaver K, Li K, Wang L, Lamm M, Zhao X, Korey M, Neivandt D, Dixon B, Sultana S, Kelly P, Gramlich WM, Tekinalp H, Gardner DJ, MacKay S, Nawaz K, Ozcan S. Pretreatment of lignocellulosic feedstocks for cellulose nanofibril production. Cellulose 2022;29:4835–76. https://doi.org/10.1007/s10570-022-04580-z.
[26] Nasir M, Hashim R, Sulaiman O, Nanocellulose M Asim. Preparation methods and applications. In: Cellulose-reinforced nanofibre composites: production, properties and applications. Woodhead Publishing; 2017. p. 261–76. https://doi.org/10.1016/B978-0-08-100957-4.00011-5.
[27] Choi K, Gao CY, Do Nam J, Choi HJ. Cellulose-based smart fluids under applied electric fields. Materials 2017;10:1060. https://doi.org/10.3390/ma10091060.
[28] Choi K, Do Nam J, Kwon SH, Choi HJ, Islam MS, Kao N. Microfibrillated cellulose suspension and its electrorheology. Polymers 2019;11:2119. https://doi.org/10.3390/polym11122119.
[29] Tilki T, Yavuz M, Karabacak Ç, Çabuk M, Ulutürk M. Investigation of electrorheological properties of biodegradable modified cellulose/corn oil suspensions. Carbohydr Res 2010;345:672–9. https://doi.org/10.1016/j.carres.2009.12.025.
[30] Muthoka RM, Panicker PS, Kim J. Molecular dynamics study of cellulose nanofiber alignment under an electric field. Polymers 2022;14:1925. https://doi.org/10.3390/polym14091925.
[31] Kadimi A, Benhamou K, Ounaies Z, Magnin A, Dufresne A, Kaddami H, Raihane M. Electric field alignment of nanofibrillated cellulose (NFC) in silicone oil: impact on electrical properties. ACS Appl Mater Interfaces 2014;6:9418–25. https://doi.org/10.1021/am501808h.
[32] Hwang S, Walker CC, Ozcan S, Tekinalp H, Han Y, Gardner DJ. Characterization of spray dried cellulose nanofibrils produced by a disk refining process at different fineness levels. Cellulose 2024;31:263–77. https://doi.org/10.1007/s10570-023-05613-x.
[33] Ogunniyi DS. Castor oil: a vital industrial raw material. Bioresour Technol 2006; 97:1086–91. https://doi.org/10.1016/j.biortech.2005.03.028.
[34] Quinchia LA, Delgado MA, Valencia C, Franco JM, Gallegos C. Viscosity modification of different vegetable oils with EVA copolymer for lubricant applications. Ind Crops Prod 2010;32:607–12. https://doi.org/10.1016/j.indcrop.2010.07.011.
[35] Kim SG, Choi HJ, Jhon MS. Preparation and characterization of phosphate cellulose-based electrorheological fluids. Macromol Chem Phys 2001;202:521–6. https://doi.org/10.1002/1521-3935(20010201)202:4<521::AID-MACP521>3.0.CO. 2-Q.
[36] Wu H, Liu H, Xue Z, Yang J, Li Q, He D, Siew WH. The generation and migration of bubbles in oil-pressboard insulation needle-plate system. IEEE Trans Dielectr Electr Insul 2022;29. https://doi.org/10.1109/TDEI.2022.3210486.
[37] García-Morales M, Fernández-Silva SD, Roman C, Olariu MA, Cidade MT, Delgado MA. Preliminary insights into electro-sensitive ecolubricants: a comparative analysis based on nanocelluloses and nanosilicates in castor oil. Processes 2020;8:1060. https://doi.org/10.3390/pr8091060.
[38] Le Bras D, Strømme M, Mihranyan A. Characterization of dielectric properties of nanocellulose from wood and algae for electrical insulator applications. J Phys Chem B 2015;119:5911–7. https://doi.org/10.1021/acs.jpcb.5b00715.
[39] Luo Q, Shen H, Zhou G, Xu X. A mini-review on the dielectric properties of cellulose and nanocellulose-based materials as electronic components. Carbohydr Polym 2023;303:120449. https://doi.org/10.1016/j.carbpol.2022.120449.
[40] Macosko CW. Rheology - principles, measurements and applications. first ed. Wiley-VCH; 1994.
[41] Parker GW. Electric field outside a parallel plate capacitor. Am J Phys 2002;70: 502–7. https://doi.org/10.1119/1.1463738.
[42] Delgado MA, Valencia C, Sánchez MC, Franco JM, Gallegos C. Thermorheological behaviour of a lithium lubricating grease. Tribol Lett 2006;23:47–54. https://doi.org/10.1007/s11249-006-9109-5.
[43] Otsubo Y. Electrorheology of whisker suspensions. In: Colloids surf A physicochem eng asp; 1999. p. 459–66. https://doi.org/10.1016/S0927-7757(98)00468-3.